Check for updates

Incorporation and electronic sensing device effects of aniline functionality in diketopyrrolopyrrole–thiophene semiconducting polymers†

Sasikumar Mayarambakam,‡[a] Christopher Riley Bond,‡[a] Howard E. Katz, [ID] *[a] Jimetochukwu Solomon[b] and Hany F. Sobhi[b]

The detection and monitoring of volatile organic compounds (VOCs) are crucial in environmental and medical monitoring. Organic field-effect transistor (OFET)-based sensors offer several advantages over conventional spectroscopic methods, including real-time, low-power, and wearable integration capabilities. In particular, diketopyrrolopyrrole (DPP)-based polymers exhibit exceptional semiconducting properties, making them promising candidates for active layers in OFET sensors. Their chemical tunability enables the incorporation of selective and sensitive biomarker moieties, either on the polymer backbone or side chains, to enhance analyte specificity. In this study, we synthesized a series of seven DPP-based copolymers functionalized with aniline derivatives named **P1**, **P2**, **P3**, **P1BT1:1**, **P1BT1:2**, **P3BT1:1** and **P3BT1:2** as biomarkers for acetone sensing. The aniline functionalities were systematically modified with electron-donating (methoxy) and electron-withdrawing (chloro) substituents to evaluate their impact on sensor performance. Device optimization was achieved by investigating different dielectric materials, including SiO_2 and cross-linked polystyrene on SiO_2, the latter effectively reducing observed gate leakage. Further optimization of the semiconducting layer was performed by comparing devices incorporating pristine aniline-functionalized DPP polymers with those utilizing a blend of pristine polymers and PDPP4T to enhance charge transport. The sensing performance of the optimized OFET devices was evaluated for acetone, dimethyl carbonate, and acetic acid, in vapor and solution phases. The findings from this study provide insights into the structure–property relationships of DPP-based semiconductors for VOC detection and highlight their potential for integration into portable electronic sensors.

Introduction

Polymer semiconductors[1–4] have emerged as promising materials for next-generation flexible,[5–8] lightweight, and low-cost electronic devices in various branches of organic optoelectronics like organic field-effect transistors (OFETs),[9–11] organic photovoltaic cells,[12–14] gas sensors,[15–20] organic light-emitting diodes,[21] organic photodetectors, *etc.* In the realm of organic electronics, OFETs[22,23] have emerged as vital components. Diketopyrrolopyrrole (DPP) has

garnered significant attention among the various building blocks utilized in designing polymeric semiconductors.[24–26] The DPP unit consists of a planar, electron-deficient heterocyclic structure that can be easily conjugated to various electron-donating or electron-withdrawing groups to tailor the electronic energy levels, bandgap, and solubility of the resulting polymers.[27] Their exceptional electronic properties, high charge-carrier mobility,[28–31] chemical stability, and structural versatility have made DPP-based polymer semiconductors ideal candidates for a wide range of applications, including organic field-effect transistors (OFETs),[32–34] organic photovoltaic cells (OPVs),[13] and gas sensors.[8] These tunable properties allow DPP-based polymers to exhibit ambipolar[35] or unipolar charge transport behavior, with substantial charge-carrier mobilities. This makes DPP-based materials attractive for developing chemical sensors.[36,37]

The interaction of DPP-based polymer thin films with target gas molecules induces measurable changes in their electronic

[a] *Department of Materials Science and Engineering, Johns Hopkins University, 206 Maryland Hall, 3400 North Charles Street, Baltimore, MD 21218, USA. E-mail: hekatz@jhu.edu*

[b] *Department of Natural Science, Center for Organic Synthesis, Coppin State University, 2500 West North Avenue, Baltimore, MD 21216-3698, USA*

† Electronic supplementary information (ESI) available. See DOI: https://doi.org/10.1039/d5tc01597a

‡ These authors contributed equally to this work.

18176 | *J. Mater. Chem. C*, 2025, **13**, 18176–18186

This journal is © The Royal Society of Chemistry 2025

properties,[38] paving the way for sensitive, selective, and cost-effective gas sensors. The interaction of volatile organic compounds (VOCs)[39] with the polymer backbone can induce significant changes in the electrical conductivity and charge transport behavior, enabling selective detection of gases such as ammonia[20] and nitrogen dioxide (NO_2),[37,39] applicable to health, food,[40] environmental monitoring, and industrial safety.

Specific functional groups having affinity for particular VOCs can enhance response thereto, where the interaction between VOC analyte molecules and the functional group can lead to measurable changes in the conductivity and charge-trapping behavior, thereby enhancing sensor sensitivity and selectivity.[41] Yao et al. synthesized a series of DPP-quaterthiophene conjugated polymers functionalized with urea groups on the alkyl side chains, exhibiting high hole mobility and enhanced photovoltaic performance.[42] Yang et al. developed a DPP-based conjugated polymer incorporating thymine moieties in the side chains, where thin films of the polymer demonstrated selective responses to CO and H_2S in the presence of Pd(II) and Hg(II) ions, respectively.[43] Yang et al. reported a thin-film field-effect transistor (FET)-based sensor for ammonia and amine detection, utilizing the DPP–bithiophene conjugated polymer, appended with tert-butoxycarbonyl-functionalized side chains.[44] Among VOCs, acetone is of great interest as an analyte for environmental monitoring, industrial safety, and medical diagnostics due to its relevance as a biomarker for various health conditions, including diabetes.[49,50] However, it is challenging to obtain a specific response to this VOC, as it is considerably less reactive than oxidizing or reducing gases that are investigated more often with conjugated polymer semiconductors.

The aniline moiety possesses electron-donating and nucleophilic characteristics (oxidation potential about +0.55 V vs. SCE or Ag/AgCl)[45] that when associated with the electron-deficient DPP unit that deepens the highest occupied molecular orbital (HOMO) levels in a semiconducting polymer (to several tenths of a volt deeper than anilines),[46] introduces localized energy levels capable of trapping holes. This hole-trapping effect plays a pivotal role in fine-tuning the charge-carrier dynamics within DPP-based thin films, impacting the overall performance of OFETs and other devices. The aniline amino group is postulated to interact with acetone and might form carbinolamine intermediates,[47,48] potentially leading to an electronic perturbation of the main chain that can be signaled in devices, as long as the hole-trapping activity does not prevent device function. It does not appear that a nucleophilic aniline, or any other amine functionality, has been appended to conjugated thiophene polymers before, and certainly not to DPP-based polymers.

This article discusses aniline-functionalized DPP-based polymer design, synthesis, and application, focusing on utilization in OFETs and gas-sensing devices. The aniline groups are on eight-carbon side chains, chosen to optimize solubility and aniline number density. We synthesized seven DPP-based co-polymers varying the substitutes on the phenyl ring in the aniline attached through the alkyl chain to the DPP.[49]

The substitutes were hydrogen, an electron-donating methoxy group, and an electron-withdrawing chloro group. We discuss the impact of aniline substitution on molecular packing, energy levels, and charge-carrier dynamics in thin films and device optimization using varying dielectric materials. Furthermore, we explore the potential of these materials in OFETs and volatile organic compound sensors, shedding light on their structure–property relationships and performance optimization strategies. By exploring the interplay between molecular functionalization, charge transport, and analyte interaction, this work aims to provide insights into developing next-generation multifunctional organic semiconductors.

Experimental

Synthesis and characterization

DPP-based co-polymers are designed so that one DPP unit contains an aniline functional group, and the other has an alkyl side chain (PDPP4T). Polymers **P1**, **P2**, and **P3** are synthesized via Stille polymerization by varying the para-H atom in the aniline moiety of the amine functional group. **P1** – contains H atoms, **P2** – contains OCH_3 groups and **P3** – contains Cl atoms. After synthesis, the polymers show limited solubility in common organic solvents like chloroform, chlorobenzene, and dichlorobenzene. Based on an initial electronic property comparison, the OCH_3 group was eliminated from further consideration, while the bithiophene units in the **P1** and **P3** are replaced with the 4-dodecyl bithiophenes to improve solubility and obtain a good film morphology. Four polymers are designed and synthesized with the retention of the **P1** and **P3** amine functionalities with dodecyl bithiophenes, altering the ratios of the amine-functionalized DPP unit and alkylated DPP unit from 1:1 to 1:2 ratio, respectively. The polymers are named **P1BT1:1**, **P1BT1:2**, **P3BT1:1**, and **P3BT1:2**. The solubility of the polymers with dodecyl bithiophenes is dramatically increased, which leads to a good film morphology. The chemical structures of the polymers are shown in Fig. 1. The synthetic scheme is depicted in the ESI† in Schemes S1–S3. The crude polymers are precipitated in methanol and subjected to Soxhlet extraction to remove short-chain polymers and unreacted monomers.

The Soxhlet extraction started with methanol, acetone, hexane, and chloroform. **P1**, **P2** and **P3** are collected from chloroform extraction, and **P1BT1:1**, **P1BT1:2**, **P3BT1:1**, and **P3BT1:2** are collected from hexane extraction, reprecipitated in methanol and the residue is collected by vacuum filtration. All the polymers are subjected to Boc deprotection in dichloromethane using trifluoroacetic acid. The polymers are dried in a vacuum oven for 2 days at 50 °C and stored in a desiccator. We also considered primary amino-terminated linear alkyl side chains on DPP-quaterthiophene repeat units. We were able to make such polymers with the amine group protected as phthalimide, but hydrazine deprotection proved unsuccessful, as the hydrazine may have reduced the DPP groups. Other protecting groups that would have given primary amines by nonreducing deprotection resulted in insoluble products.
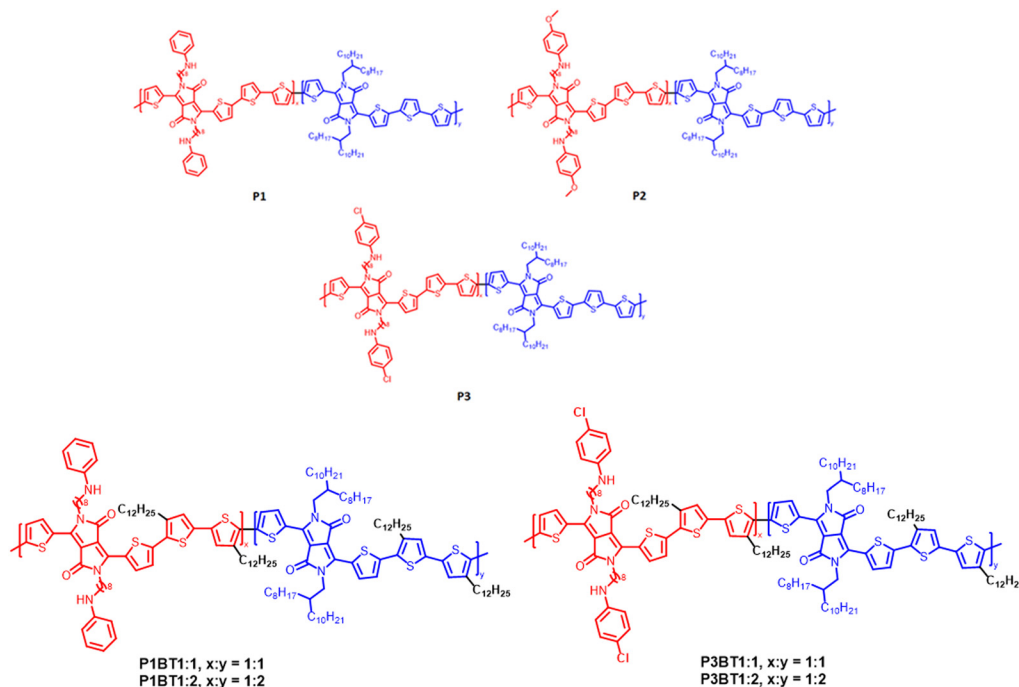
This journal is © The Royal Society of Chemistry 2025

J. Mater. Chem. C, 2025, 13, 18176–18186 | 18177

Fig. 1 Chemical structures of polymers **P1**, **P2**, **P3**, **P1BT1:1**, **P1BT1:2**, **P3BT1:1** and **P3BT1:2**.

Optical, electrochemical, and thermal properties

The normalized UV-vis absorption spectra of polymers are depicted in Fig. 2(a), and the results are summarized in Table 1. The chloroform solutions of the polymers are used to obtain solution state UV-vis spectroscopy. All the polymers showed two distinct peaks in the range 409–421 nm and
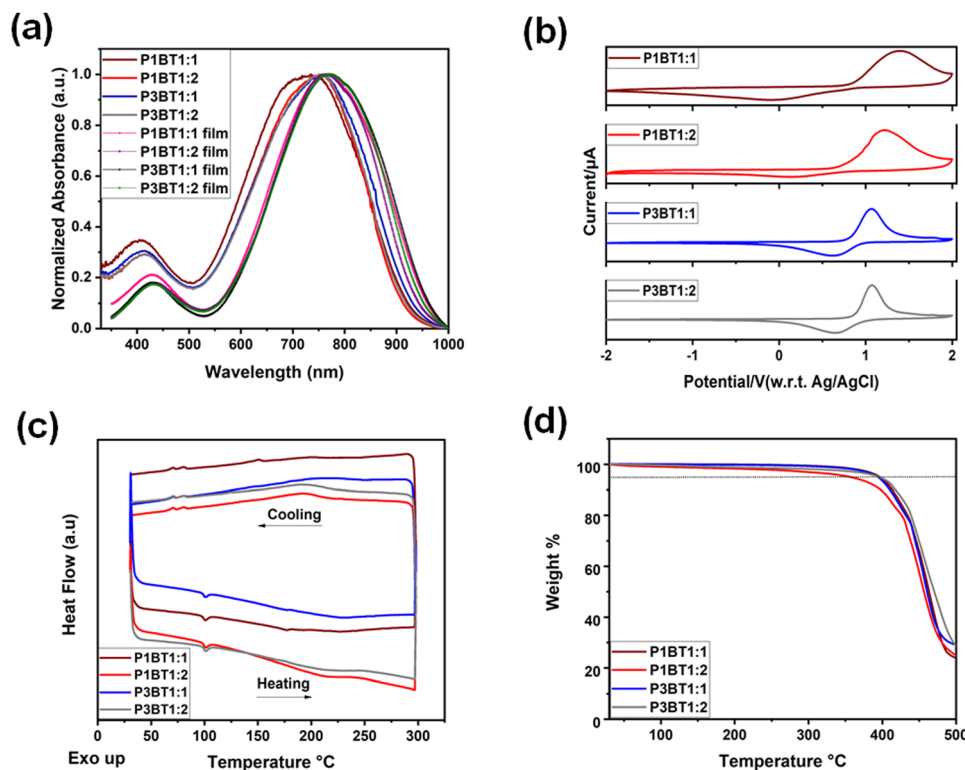

Fig. 2 (a) Normalized UV-vis absorption spectra in solution and thin film states, (b) cyclic voltammograms recorded on a drop-cast film, (c) DSC second heating and cooling cycles and (d) TGA thermograms of polymers **P1BT1:1**, **P1BT1:2**, **P3BT1:1** and **P3BT1:2**.

18178 | *J. Mater. Chem. C*, 2025, **13**, 18176–18186

This journal is © The Royal Society of Chemistry 2025

Paper

Table 1 Optical and electrochemical properties of polymers

Polymers	Optical data			Electrochemical data		
	$\lambda_{max, sol.}$[a] (nm)	$\lambda_{max, film}$[b] (nm)	E_g[c] (eV)	$E_{1/2ox}$[d] (V)	HOMO[e] (eV)	LUMO[f] (eV)
P1BT1:1	409, 734	430, 765	1.34	0.50	−5.30	−3.96
P1BT1:2	424, 745	434, 764	1.37	0.40	−5.20	−3.83
P3BT1:1	414, 755	428, 769	1.33	0.46	−5.26	−3.93
P3BT1:2	421, 751	434, 772	1.34	0.52	−5.32	−3.98

[a] Absorption peaks in chloroform solution. [b] Absorption peaks of polymer thin films spin-coated from chloroform solution. [c] The optical band gap, determined from Tauc plots (provided in Fig. S3, ESI), was calculated using the absorption coefficient derived from thin films. [d] Onset oxidation potentials after correction relative to ferrocene. [e] HOMO energy calculated from HOMO = $-e(E_{ox} + 4.8)$ (eV). [f] LUMO energy calculated from LUMO = (HOMO − Bandgap) (eV).

734–755 nm. The peak in the lower wavelength corresponds to the π–$\pi^\star$ transition of the bithiophene units. A few nm of bathochromic shift is observed in the maximum wavelength region of **P3BT1:1** and **P3BT1:2** compared to **P1BT1:1** and **P1BT1:2**. In the thin film state, all polymers exhibited maximum absorption bands in the range of 763–772 nm. The observed bathochromic shift in the thin film spectra compared to the solution state is attributed to the intermolecular interaction and aggregation in the film state. **P3BT1:2** exhibits the highest λ_{max} among all the polymers in the thin film state; however, in comparison to its counterpart **P3BT1:1**, the shift is a few nanometers. **P1BT1:1**, **P1BT1:2**, **P3BT1:1**, and **P3BT1:2** are shown to have 31 nm, 18 nm, 14 nm and 21 nm redshifts in the film state compared to their solution state, respectively.

Cyclic voltammetry measurements were performed on polymers using a three-electrode system to study the electrochemical behavior. The results are depicted in Fig. 2(b). Polymer solution in chloroform was drop-cast onto the glassy carbon working electrode. Measurements were performed at room temperature using an Ag/AgCl reference, a glassy carbon working electrode and a Pt wire counter electrode in 0.1 M tetrabutylammonium perchlorate as the supporting electrolyte in acetonitrile. Tests were performed with a scan rate of 0.1 V s^{-1}, and the tests were calibrated using a ferrocene/ferrocenium redox couple. All the polymers showed oxidation potentials from 0.8 to 0.86 V vs. Ag/AgCl, in agreement with literature values for PDPP4T.[50] No redox peaks were observed for any polymers. The highest occupied molecular orbital (HOMO) values are calculated from the onset of oxidation potentials after correcting to ferrocene and are listed in Table 1. **P3BT1:1** and **P3BT1:2** showed a one-electron reversible oxidation cycle; however, in **P1BT1:1** and **P1BT1:2**, the reversible cathodic peak is diminished.

The presence of the chloro group has minimal or no effect on the HOMO energy levels of P3BT polymers, though it does affect the electron donating capability of the anilines themselves. All polymers showed similar onset oxidation potentials, indicating little effect of backbone ratio alterations on oxidation potentials.

Differential scanning calorimetry (DSC) studies were performed to evaluate the thermal properties of polymers. The DSC traces are presented in Fig. 2(c) and Fig. S2, ESI.† All polymers show two glass

transition (T_g) temperatures. The first T_g is attributed to the alkylated DPP unit, and the second transition could be attributed to the amine-functionalized DPP unit. The second transition in **P1BT1:1** and **P3BT1:1** is seen due to the equal ratios of amine-functionalized and alkyl-chain-functionalized DPP units. However, in polymers **P1BT1:2** and **P3BT1:2**, the second transition is decreased and remains unclear because the ratio of the amine-functionalized DPP is lower than that of the alkylated DPP unit. Polymers **P1**, **P2**, and **P3** showed the first transition around 102 °C and the second in the 203–205 °C range and are presented in Table S1 (ESI†). Polymers **P1BT1:1**, **P1BT1:2**, **P3BT1:1**, and **P3BT1:2** showed the first and second transition temperatures around 99 °C and 177 °C, respectively. The C-12 alkyl chains on the bithiophenes in **P1BT1:1**, **P1BT1:2**, **P3BT1:1**, and **P3BT1:2** make polymers less crystalline than **P1**, **P2**, and **P3**, leading to a decrease in the glass transition temperatures. Thermogravimetric analysis of the polymers revealed that all the polymers possess excellent thermal stability. The thermal stability of polymer semiconductors is an important parameter that allows the use of different deposition techniques other than solution deposition techniques like spin coating or drop-casting. All polymers showed high decomposition temperatures T_d, (defined as the temperature at which 5 wt% loss is observed). The observed thermal stability of the polymers suggests a minimal possibility of degradation and molecular deformations during device fabrication and opens for vacuum deposition techniques. **P1BT1:1**, **P1BT1:2**, **P3BT1:1**, and **P3BT1:2** showed decomposition temperatures of 395, 360, 394 and 396 °C, respectively. **P3BT1:2** shows the highest T_d, suggesting it is thermally more stable than the other polymers. The TGA thermograms are shown in Fig. 2(d), and the results are depicted in Table S1 (ESI†).

Electronic properties and responses

The output and transfer characteristics of each OFET were measured to assess the quality of transistor behavior in each sample along with their stability and reproducibility and are shown in Fig. 3 for OFETs comprising PDPP4T, **P1BT1:1**, or **P3BT1:1** active layers on XLPS/SiO$_2$ gate dielectrics. Additional output and transfer characteristics of all measured OFETs, including OFETs comprising SiO$_2$ gate dielectrics for **P1**, **P2** and **P3** with no XLPS, are provided in Fig. S8–S14 of the ESI.†

OFETs comprising **P1BT1:1**, **P1BT1:2**, **P3BT1:1**, and **P3BT1:2** on XLPS/SiO$_2$ gate dielectrics show clear signs of shallow trapping by the aniline groups. While the threshold voltages are similar, the gate-induced current increments are significantly less for the aniline-containing polymers. This may be an inevitable effect of attempting to use a nucleophilic binding group in an OFET detection mechanism.

After determining OFET characteristics, device responses to various concentrations of acetone gas were assessed. Before exposing a device to acetone gas, the drift current was determined by measuring 25 transfer curves at a rate of −10 V s^{-1} with the device exposed to air under ambient conditions, where I_{ds} was measured as a function of V_g from 0 to −50 V with V_{ds} held constant at −50 V. Upon completion of the drift current

This journal is © The Royal Society of Chemistry 2025

J. Mater. Chem. C, 2025, **13**, 18176–18186 | **18179**
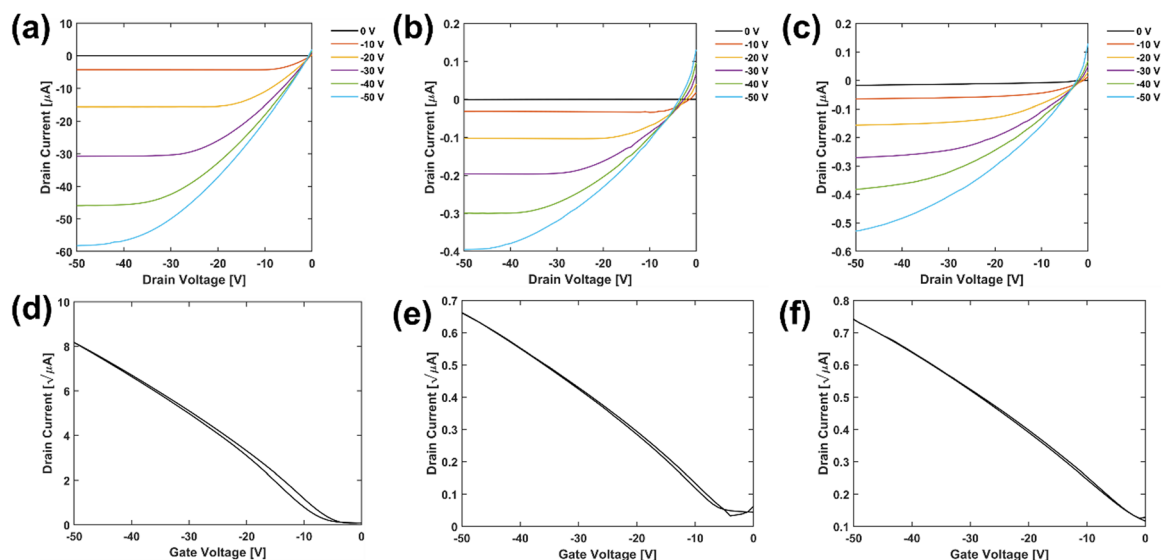
Fig. 3 The output characteristics of OFETs comprising (a) PDPP4T on XLPS/SiO$_2$, (b) **P1BT1:1** on XLPS/SiO$_2$, and (c) **P3BT1:1** on XLPS/SiO$_2$, and the square root transfer characteristics of OFETs comprising (d) PDPP4T on XLPS/SiO$_2$, (e) **P1BT1:1** on XLPS/SiO$_2$, and (f) **P3BT1:1** on XLPS/SiO$_2$.

measurement, the device was immediately exposed to acetone gas in a closed chamber with transfer curves measured every 3 minutes under conditions identical to those used for the drift measurement. The initial concentration of acetone gas was held at 5 ppm, and once a transfer curve was recorded after 3 minutes of exposure, the process was repeated for concentrations of 10, 20, and 50 ppm of acetone gas. The results of the acetone sensitivity measurements are shown in Fig. 4, with additional transfer curves showing OFET drift currents and responses to acetone gas available in Fig. S14–S17 of the ESI.† Limits of detection ranged from 0.043 ppm for P1BT:PDPP4T to 1–16 ppm for the others, as shown and explained in Fig. S31, ESI.† In addition to measuring the responses of OFETs to acetone gas, the changes in transfer characteristics of each OFET were measured when exposed to solutions of various analytes in 2-propanol (IPA).[51] Solutions with concentrations of 1 µg analyte/1 mL IPA, 10 µg analyte/1 mL IPA, and 100 µg analyte/1 mL IPA were prepared for the analytes, acetic acid (AA), dimethyl carbonate (DMC), and acetone to produce a total of nine unique solutions.

To test OFET responses to each analyte, an initial transfer curve was recorded using previously described measurement conditions, followed by distribution of 1.5 µL of pure IPA with no analyte in the OFET channel using a 100 µL pipette tip. The IPA was allowed to completely evaporate until no liquid remained in the OFET channel, upon which a second transfer curve was immediately recorded under identical measurement conditions. This process was then repeated three times for a given analyte, where 1.5 µL of the 1 µg analyte/1 mL IPA solution was evaporated in the OFET channel and a new transfer curve was immediately recorded, followed by 1.5 µL of the 10 µg analyte/1 mL of IPA solution and lastly 1.5 µL of the 100 µg analyte/1 mL of IPA solution. A unique OFET was used for measuring the response to each type of analyte solution to avoid contamination and conflicting device responses.

The sensitivity of select OFETs to IPA and each of the three analytes are shown in Fig. 5, with transfer curves showing OFET responses to each analyte and additional OFET sensitivities provided in Fig. S18–S25 of the ESI.† To further characterize the charge trapping behavior of the aniline groups in the functionalized semiconducting polymers, a series of two-terminal measurements were conducted on each OFET. Starting with a constant V_g of 0 V, 25 consecutive scans of I_{ds} were measured as a function of V_{ds} from 50 V to −50 V. The same protocol was then repeated with V_g set to −25 V and subsequently +25 V to produce three sets of 25 curves measured at three unique gate biases. The results of the two-terminal measurements at each of the three gate biases for two OFETs are shown in Fig. 6, with additional OFET two-terminal measurement results provided in Fig. S26–S30 of the ESI.†

Discussion and analysis

The inclusion of aniline groups in the semiconductor layer of each OFET causes modest changes in the quality of the output and transfer behavior, as shown in Fig. 3. OFETs comprising PDPP4T on XLPS/SiO$_2$ gate dielectrics show ideal transistor behavior with large I_{ds}, high mobility, and very small leakage currents. There are slight effects of contact resistance present in the output characteristic,[52] but they are minimized up to a V_g of −40 V. OFETs comprising aniline-functionalized semiconducting polymers exhibit decreased I_{ds}, lower mobilities, and larger leakage currents, with similar effects of contact resistance observed in the output characteristics.

The decrease in I_{ds} observed in both the output and transfer characteristics of OFETs comprising aniline-functionalized semiconducting polymers is due to the hole trapping characteristics of the aniline groups.[53,54] The greater concentration of aniline leads to increased hole trapping and consequently
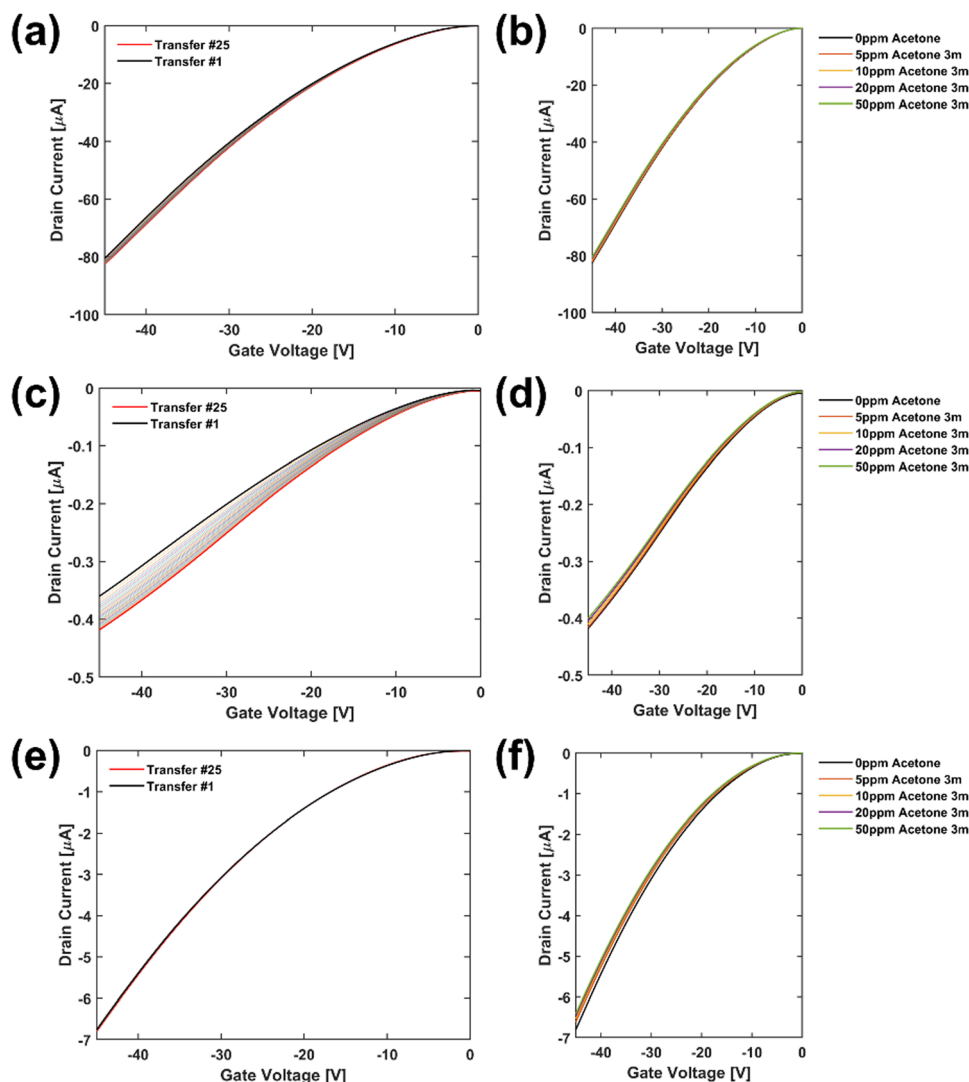
18180 | *J. Mater. Chem. C*, 2025, **13**, 18176–18186

This journal is © The Royal Society of Chemistry 2025

Fig. 4 PDPP4T on XLPS/SiO$_2$ OFETs: (a) drift current in air and (b) response to acetone gas exposure. **P3BT1:2** on XLPS/SiO$_2$ OFETs: (c) drift current in air and (d) response to acetone gas exposure. P1BT : PDPP4T blend (25 : 75 by weight) on XLPS/SiO$_2$ OFETs (e) drift current in air and (f) response to acetone gas exposure.
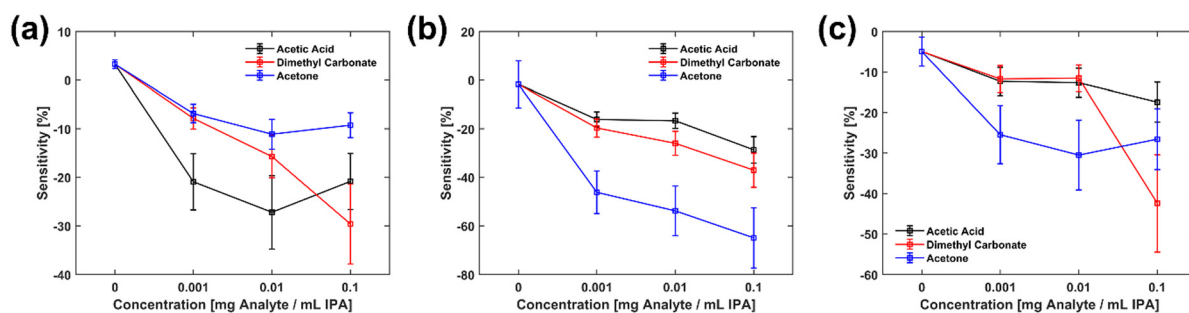

Fig. 5 Responses to analyte in IPA solutions of (a) PDPP4T on XLPS/SiO$_2$ OFETs, (b) **P1BT1:1** on XLPS/SiO$_2$ OFETs, and (c) P3BT : PDPP4T blend (25 : 75 by weight) on XLPS/SiO$_2$ OFETs. Error bars are standard deviations from three measurements per point.

smaller currents, which is clearly observable when comparing samples such as **P1BT1:2**, **P1BT1:1**, and **P1BT1:1** blended with PDPP4T in a 25 : 75 ratio by weight. The blended sample exhibits the largest maximum I_{ds} of −13 µA due to the lowest concentration of hole trapping aniline groups being present, while samples with 33% and 50% functionalization and no
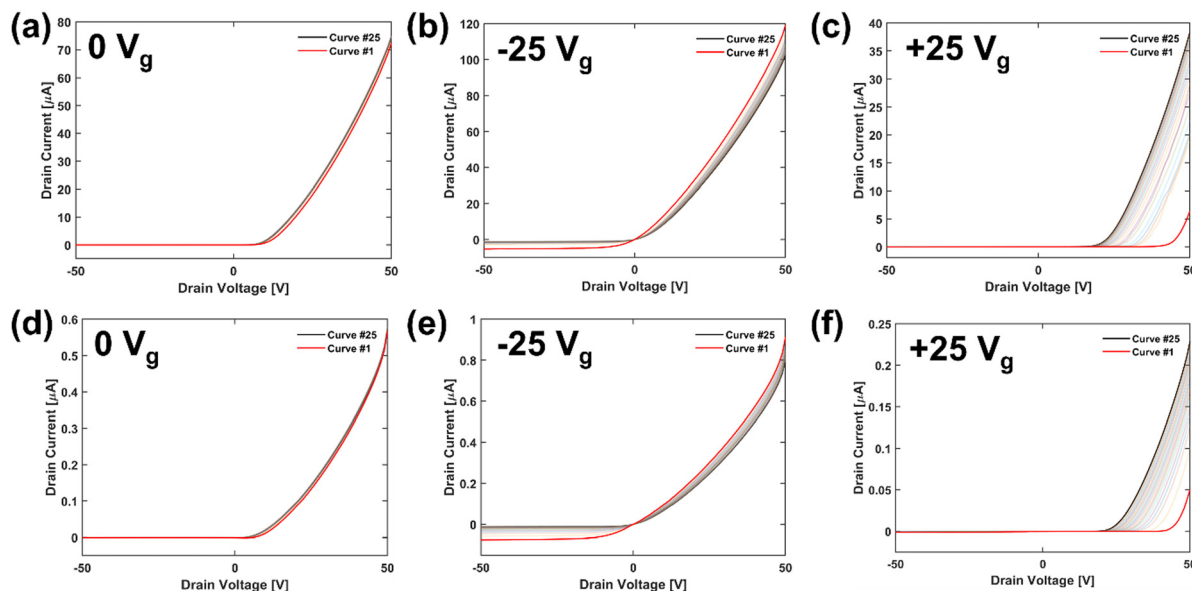
Fig. 6 Two-terminal measurements of PDPP4T on XLPS/SiO$_2$ OFETs with gate biases of (a) 0 V, (b) −25 V, and (c) +25 V. Two-terminal measurements of **P1BT1:1** on XLPS/SiO$_2$ OFETs with gate biases of (d) 0 V, (e) −25 V, and (f) +25 V.

blended PDPP4T exhibit currents two orders of magnitude smaller at −800 nA and −400 nA, respectively. The same comparison can clearly be made when considering the transfer characteristics of these devices, where similar differences in I_{ds} magnitude are observable.

Due to the aniline groups producing observable current decreases in the output and transfer characteristics of OFETs, the leakage current of devices comprising these polymers is relatively more prominent than for pure PDPP4T OFETs. The magnitude of the leakage current is similar for all devices on the order of 200 nA, yet it is only clearly observable in the characteristics of devices not containing PDPP4T. OFETs containing PDPP4T exhibit maximum I_{ds} more than 100 times greater than the leakage current, while those without PDPP4T and containing aniline-functionalization exhibit a maximum I_{ds} just 5 to 10 times greater than the leakage current. In addition to leakage current being more prominent in aniline-functionalized OFETs, a significant decrease in device mobility is also observable as tabulated in Table 2. These mobilities were calculated from the transfer characteristics of each OFET using the following equation: $I_{ds} = \frac{W}{2L}\mu C(V_g - V_{th})^2$, where W is the channel width of the OFET, L is the channel length of the OFET, μ is the hole mobility of the OFET, C is the measured capacitance per unit area of the OFET, and V_{th} is the threshold voltage.[55] The mobility of PDPP4T on XLPS/SiO$_2$ OFETs was determined to be 0.25 ± 0.01 cm^2 V^{-1} s^{-1}, while blending in just 25% by weight of **P1BT1:1** reduces the mobility more than 10 times to $0.23 \times 10^{-1} \pm 0.09 \times 10^{-1}$ cm^2 V^{-1} s^{-1}. A similar order of magnitude decrease in mobility is observed when blending 25% by weight of **P3BT1:1** with PDPP4T, while OFETs comprising aniline-functionalized semiconductors with no PDPP4T exhibit mobilities two orders of magnitude smaller than pure PDPP4T OFETs due to the strong hole trapping characteristics of the functionalized aniline groups.

Table 2 Active layer, threshold voltage, capacitance, and hole mobility of measured OFETs. Three devices were measured to obtain each parameter

Active layer	V_{th} (V)	C (pF)	μ (cm^2 V^{-1} s^{-1})
PDPP4T	-4.1 ± 0.1	430 ± 17	0.25 ± 0.01
P1BT1:1	-1.2 ± 0.3	400 ± 10	$0.15 \times 10^{-2} \pm 0.01 \times 10^{-2}$
P1BT1:2	0.84 ± 0.18	410 ± 25	$0.29 \times 10^{-2} \pm 0.02 \times 10^{-2}$
P1BT:PDPP4T	0.17 ± 0.22	560 ± 20	$0.23 \times 10^{-1} \pm 0.09 \times 10^{-1}$
P3BT1:1	7.1 ± 0.6	440 ± 60	$0.13 \times 10^{-2} \pm 0.02 \times 10^{-2}$
P3BT1:2	2.2 ± 0.8	450 ± 70	$0.16 \times 10^{-2} \pm 0.02 \times 10^{-2}$
P3BT:PDPP4T	0.64 ± 0.11	520 ± 50	$0.26 \times 10^{-1} \pm 0.02 \times 10^{-1}$

While the OFET characteristics of devices comprising XLPS/SiO$_2$ dielectrics are stable and reproducible, this is not the case for dielectrics comprising only SiO$_2$. When a polymer other than PDPP4T is deposited on SiO$_2$, initial OFET characteristics can be measured, albeit with far less ideal results than what is shown in Fig. 3. The quality of these characteristics rapidly degrades with repeated measurements, with OFETs becoming immeasurable after just a few measurements are performed. This irreversible failure of the devices is likely due to the aniline groups of the functionalized polymers reacting with the oxide dielectric.[53,54,56] This failure is also not dependent on the total number of measurements performed on a device, as a given device could be measured once, stored under a vacuum for a short period of time, and then be immeasurable once removed from storage due to the amine-oxide reaction. As a result of the discovery of this failure mechanism, P1BT and P3BT OFETs were only fabricated on XLPS/SiO$_2$ dielectrics, as the introduction of XLPS to separate the aniline groups from the oxide completely resolved this observed failure mechanism. **P1, P2**, and **P3** could not produce measurable OFETs on the XLPS/SiO$_2$ dielectric due to a lack of solvent compatibility hindering the deposition of a continuous semiconducting layer atop the XLPS layer.

18182 | J. Mater. Chem. C, 2025, **13**, 18176–18186

This journal is © The Royal Society of Chemistry 2025

Paper

P2 was not further functionalized to enable use on XLPS/SiO$_2$ due to extreme charge trapping and instability when deposited on SiO$_2$, consistent with the easier oxidizability of oxyanilines[57] compared to the other two. Despite the modest stabilization against oxidation offered by the chloro group, the chlorinated aniline derivative P3BT showed better-behaved cyclic voltammograms than P1BT, while their OFET characteristics were similar.

In addition to observing failure when functionalized polymers were deposited on dielectrics comprising only SiO$_2$, failure was also observed in devices comprising functionalized polymers deposited on XLPS/SiO$_2$ after exposure to acetone gas. While the largest responses in acetone gas could be observed in XLPS/SiO$_2$ OFETs comprising **P3BT1 : 2** and a 25 : 75 by weight blend of P1BT : PDPP4T, the measurement results could not be reproduced by the same OFETs that generated these responses. After exposing these devices to acetone gas at concentrations of 5, 10, 20, and 50 ppm for three minutes each, the devices were placed under a vacuum at 50 °C for 30 minutes to remove any remaining acetone gas, attempting to reset the device to baseline characteristics for additional sensing experiments. However, when an attempt was made to repeat the sensitivity measurement on the same device, that device proved immeasurable, and baseline transfer characteristics could not be obtained. This observation held for all devices containing any aniline functionalization, where the sensitivity of a given OFET could be measured at each concentration of acetone gas once but would not be measurable the second time. It is possible that this failure occurs due to an irreversible reaction between the aniline groups and acetone that forms carbinolamine in the active layer of the OFETs.[58] To obtain an average acetone response value with uncertainty values for each exposure concentration, three unique batches of devices for each type of OFET had to be fabricated and independently tested due to this failure mechanism. Additionally, the failure did not seem to be dependent on the concentration of acetone gas, but it rather depended on the duration of exposure to acetone gas. Thus, the materials could function in one-time detectors of acetone but would not be suitable for continuous monitoring. Efforts to attain reversible strong responses to acetone from such semiconducting polymers are ongoing.

In general, while responses to acetone gas of all devices on XLPS/SiO$_2$ dielectrics are modest, they are apparently enhanced by the aniline functionality. As mentioned above, devices comprising **P3BT1:2** and a 25:75 by weight blend of P1BT:PDPP4T exhibit the largest absolute responses to acetone gas, with maximum responses of $-4.3 \pm 1.9\%$ and $-5.8 \pm 3.3\%$, respectively, occurring in response to 50 ppm of acetone gas. Both devices exhibit more significant responses to acetone gas than do PDPP4T on XLPS/SiO$_2$, which shows only a $-2.5 \pm 1.0\%$ change in current when exposed to 50 ppm acetone gas. This results in a p-value of 0.077 for the **P3BT1:2** device and a p-value of 0.051 for the blended device for the response differences between these polymers and PDPP4T occurring by random chance when taking into account responses at all four concentrations of acetone gas.

Because the current drifts in air were in the opposite direction as the current responses to acetone, the effect of acetone is actually higher than what is indicated by the absolute responses. To correct the acetone responses for the drift, we did the following data analysis. Using the 25 transfer curves scanned in air, I_{ds} was plotted as a function of time for a fixed V_g. A linear line of best fit was applied to the current–time plot for times where I_{ds} no longer showed non-linear dependence on the measurement time. This line of best fit was then used to project I_{ds} to a longer timescale to account for the total exposure time to acetone gas at each measured concentration. The projected I_{ds} was then used to calculate the sensitivity of each device to each concentration of acetone gas, resulting in a "corrected response" that accounts for shifts in I_{ds} for drift in air and acetone gas response being in opposite directions. Table 3 lists the observed drift over three minutes in air, the concentration at which the first measurable acetone response was recorded, the time it took to complete that exposure after starting the series of exposures, the observed response, and a response corrected for the drift, as absolute percentages and as percent per ppm.

It can be observed that two of the aniline polymers, **P3BT1:2** and **P1BT1:1**, showed significantly higher normalized responses, corrected for drift, than did PDPP4T itself. Furthermore, the P1BT:PDPP4T blend (25:75) showed the highest uncorrected response because it had the lowest drift. Regardless of the magnitude of device response or the direction of shift in current, no devices could be remeasured once exposed to acetone gas except for pure PDPP4T OFETs, indicating instability associated with anilines responding to acetone that is not present in the unfunctionalized (but less responsive) PDPP4T.

Table 3 Responses to acetone corrected for drift and normalized to concentration

Figure	Polymer	Drift (%)	Acetone conc. (ppm)	Total exposure time (min)	Observed response	Observed response (%/ppm)	Corrected response (%)	Corrected response (%/ppm)
Fig. 4(a) and (b)	PDPP4T	2.55	10	6	−1.0	−0.10	−3.96	−0.40
Fig. 4(c) and (d)	**P3BT1:2**	16.16	5	3	−0.8	−0.16	−8.53	−1.71
Fig. 4(e) and (f)	P1BT : PDPP4T blend (25 : 75)	0.59	10	6	−4.0	−0.40	−5.37	−0.54
Fig. S14a and b (ESI)	**P1BT1:1**	−1.68	5	3	−1.05	−0.21	−11.65	−2.33
Fig. S15a and b (ESI)	**P3BT1:1**	8.49	20	9	−0.4	−0.02	−11.68	−0.58
Fig. S16a and b (ESI)	P3BT:PDPP4T	1.49	10	6	−0.2	−0.02	−2.20	−0.22

Responses of functionalized OFETs to solutions of acetone when delivered by IPA are far larger than their responses to acetone gas. Fig. 5 shows **P1BT1:1** on XLPS/SiO$_2$ OFETs exhibiting a response of −45% to −65% for solutions of 1 µg to 100 µg of acetone per 1 mL IPA. The maximum response of this device to 50 ppm of acetone gas, however, is only −3%. Increases in response to acetone when in a solution of IPA rather than a gas are not proportional among the materials, as PDPP4T on XLPS/SiO$_2$ OFETs exhibit a maximum response of just −10% to the 10 µg acetone/1 mL IPA solution compared to a maximum response of −2% to 50 ppm acetone gas. In this case, the aniline functionalized OFETs show an increase in maximum sensitivity of more than 20 times when exposed to the acetone solution rather than acetone gas, while PDPP4T OFETs only show a maximum sensitivity increase of 5 times. Shown in Fig. 5, the P3BT:PDPP4T blended OFETs exhibited the smallest response to acetone of all functionalized OFETs, with a maximum sensitivity of −30% to the acetone in the 10 µg acetone/1 mL of IPA solution. While this is the smallest response observed of all functionalized OFETs, it is still 3 times greater than the maximum response of the PDPP4T OFET with no aniline functionalization. Despite the improved sensitivity to acetone exhibited by functionalized OFETs when exposed to a solution rather than a gas, similar failure was still observed after the completion of the sensitivity measurement.

The vapor pressure of pure acetone is about 200 torr at room temperature. The vapor pressure of 10 ppm acetone in a noninteracting solution would be 10^{-5} times lower, about 2×10^{-3} torr if the solvent and acetone molecular weights are similar, which is the case for isopropanol as the solvent. This is an upper limit of the activity of the acetone (equivalent to partial pressure)—the activity could be further decreased in an interacting solvent (like isopropanol). An example of such decreased activity at low acetone concentrations in a hydroxylated medium has been described.[59] The partial pressure of 10 ppm acetone gas is about 760×10^{-5} torr, or about 8×10^{-3} torr, if it is ppm by moles or volume, or 4×10^{-3} torr if by weight, since there would be half as many moles of acetone in equal weights of acetone and air. Thus, the activity of the acetone is actually somewhat lower in isopropanol than in the chamber. The increased signal in isopropanol might arise, for example, from the solvent swelling the polymer and decreasing the packing density of polymer subunits, or increasing the proximity of aniline groups to the polymer interface relative to the vapor phase.

OFET responses to solutions of DMC in IPA and AA in IPA were also measured to investigate the selectivity of responses to solutions in IPA. All OFETs showed relatively small responses to pure IPA of 10% or less while exhibiting responses to analytes significantly larger than to pure IPA. PDPP4T on XLPS/SiO$_2$ OFETs showed the greatest initial response to AA and greatest maximum response to 100 µg DMC/1 mL of IPA; responses to both DMC and AA at all three solution concentrations were larger than responses to acetone, with significantly larger responses to DMC and AA at the two highest solution concentrations. In contrast to PDPP4T OFETs, all functionalized OFETs exhibited the greatest responses to acetone at all solution concentrations with a single exception shown in Fig. C, where P3BT:PDPP4T blended OFETs had a greater response to 100 µg DMC/1 mL of IPA than 100 µg acetone/1 mL of IPA. This may be because of the greater retention of the larger amount of DMC in the liquid phase with this higher deposition quantity, compared to acetone. Aniline-functionalized OFETs show sensitivity to acetone solutions 3 to 6 times greater than PDPP4T OFETs, while responses to AA and DMC are similar for all OFETs regardless of functionalization. Provided that unfunctionalized PDPP4T responds strongly to AA and DMC in IPA with little response to acetone while aniline functionalized OFETs exhibit similar responses to AA and DMC in IPA with much stronger responses to acetone, the aniline functional groups appear selective towards acetone while serving to enhance acetone sensitivity.

Two-terminal measurements conducted on each device give insight into the charge trapping behavior of the aniline groups. Depending on whether an accumulation or depletion bias is applied to the OFET gate, currents in the positive V_{ds} regime can decrease or increase with repeated measurement scans. Shown in Fig. 6, the PDPP4T on XLPS/SiO$_2$ OFET exhibits a current increase larger than 500% when a depletion bias is applied to the gate, while the **P1BT1:1** on XLPS/SiO$_2$ OFET exhibits a current increase of only 300% under the same bias. While currents in the **P1BT1:1** OFET are two orders of magnitude smaller than those in the PDPP4T OFET to begin with, smaller relative shifts in current observed under an applied depletion bias indicate a decrease in bias stress in the **P1BT1:1** device due to trapped charges being present before beginning the two-terminal measurement.[60–62] This effect is even more prominent in OFETs comprising functionalized polymers shown in the ESI,† which exhibit smaller shifts in current under an applied depletion bias due to the strong charge trapping of the aniline groups.

Conclusions

We designed and synthesized a series of seven DPP-based copolymers, each functionalized with an aniline amine group while systematically varying the *para*-position substituent from methoxy to chlorine. The initial polymers **P1**, **P2**, and **P3** exhibited poor solubility, which was addressed by incorporating long C-12 alkyl chains into the bithiophene units, leading to the development of the P1BT and P3BT polymer series. Furthermore, the ratio of amine-functionalized to alkyl-functionalized DPP units was adjusted to 1:1 and 1:2, resulting in four additional polymers: **P1BT1:1**, **P1BT1:2**, **P3BT1:1**, and **P3BT1:2**. These polymers were thoroughly characterized using UV-vis spectroscopy, cyclic voltammetry, differential scanning calorimetry (DSC), and thermogravimetric analysis (TGA) to evaluate their optical, electrochemical, and thermal properties. Bottom-gate/top-contact OFETs were fabricated using the synthesized polymers as semiconducting layers. Additionally, OFETs incorporating pristine PDPP4T and its blends with the synthesized polymers were tested for their electrical characteristics. OFETs based on PDPP4T on

18184 | J. Mater. Chem. C, 2025, 13, 18176–18186

This journal is © The Royal Society of Chemistry 2025

XLPS/SiO$_2$ attained a hole mobility of 0.25 ± 0.01 cm^2 V^{-1} s^{-1}, while the hole-trapping activity of the aniline group decreased the mobility by 1–2 orders of magnitude. Beyond OFET applications, the pristine polymers and their blends with PDPP4T were evaluated for VOC sensing, specifically for acetic acid, dimethyl carbonate, and acetone. Notably, **P3BT1:2** and a 25:75 (by weight) blend of P1BT:PDPP4T exhibited the highest response to 50 ppm acetone gas, with signal changes of $-4.3 \pm 1.9\%$ and $-5.8 \pm 3.3\%$, respectively, and reached *ca.* -10% if corrected for environmental drift. Responses several times higher were still observed from solutions of acetone in IPA, despite the activities of the acetone in those solutions being decreased compared to activities of equivalent acetone concentrations in air. These responses were also generally stronger than those to alternative carbonyl compounds acetic acid and dimethyl carbonate.

Conflicts of interest

The authors declare no conflict of interest.

Data availability

The data supporting this article have been included as part of the ESI.†

Acknowledgements

Notes and references

1 D. Zhang, C. Li, G. Zhang, J. Tian and Z. Liu, *Acc. Chem. Res.*, 2024, **57**, 625–635.

2 N. Li, Y. Li, Z. Cheng, Y. Liu, Y. Dai, S. Kang, S. Li, N. Shan, S. Wai, A. Ziaja, Y. Wang, J. Strzalka, W. Liu, C. Zhang, X. Gu, J. A. Hubbell, B. Tian and S. Wang, *Science*, 2023, **381**, 686–693.

3 J. Huang and G. Yu, *Chem. Mater.*, 2021, **33**, 1513–1539.

4 L. Ding, Z. Yu, X. Wang, Z. Yao, Y. Lü, C. Yang, J. Wang and J. Pei, *Chem. Rev.*, 2023, **123**, 7421–7497.

5 X. Zhang, Z. Pu, X. Su, C. Li, H. Zheng and D. Li, *Anal. Bioanal. Chem.*, 2023, **415**, 1607–1625.

6 S. Yuvaraja, A. Nawaz, Q. Liu, D. P. Dubal, S. G. Surya, K. N. Salama and P. Sonar, *Chem. Soc. Rev.*, 2020, **49**, 3423–3460.

7 A. Nawaz, L. Merces, L. M. M. Ferro, P. Sonar and C. C. B. Bufon, *Adv. Mater.*, 2022, **35**, 2204804.

8 F. A. Viola, A. Spanu, P. C. Ricci, A. Bonfiglio and P. Cosseddu, *Sci. Rep.*, 2018, **8**, 10824.

9 X. Wu, S. Mao, J. Chen and J. Huang, *Adv. Mater.*, 2018, **30**, 1705642.

10 L. Shi, Y. Guo, W. Hu and Y. Liu, *Mater. Chem. Front.*, 2017, **1**, 2423–2456.

11 H. Sirringhaus, *Adv. Mater.*, 2005, **17**, 2411–2425.

12 W. Li, K. H. Hendriks, M. M. Wienk and R. A. J. Janssen, *Acc. Chem. Res.*, 2016, **49**, 78–85.

13 S. Qu and H. Tian, *Chem. Commun.*, 2012, **48**, 3039–3051.

14 Y. Li, P. Sonar, L. Murphy and W. Hong, *Energy Environ. Sci.*, 2013, **6**, 1684–1710.

15 H. J. Cheon, X. Li, Y. J. Jeong, M. J. Sung, Z. Li, I. Jeon, X. Tang, H. G. Girma, H. Kong, S. K. Kwon, T. K. An, S. H. Kim and Y.-H. Kim, *J. Mater. Chem. C*, 2020, **8**, 8410–8419.

16 X. Zhang, Z. Pu, X. Su, C. Li, H. Zheng and D. Li, A Wide Dynamic Detection Range Glucose Sensor by Synergetic two P+N Organic Field-Effect Transistors, *2022 IEEE 35th International Conference on Micro Electro Mechanical Systems Conference (MEMS)*, Tokyo, Japan, 2022, pp. 301–304, DOI: **10.1109/MEMS51670.2022.9699468**.

17 E. S. Shin, J. Y. Go, G. S. Ryu, F. Shan, G. Liu and Y.-Y. Noh, *ACS Appl. Mater. Interfaces*, 2021, **13**, 4278–4283.

18 T. Someya, T. Sekitani, S. Iba, Y. Kato, H. Kawaguchi and T. Sakurai, *Proc. Natl. Acad. Sci. U. S. A.*, 2004, **101**, 9966–9970.

19 K. Besar, J. Dailey and H. E. Katz, *ACS Appl. Mater. Interfaces*, 2017, **9**, 1173–1177.

20 H. Liang, Y. Zhu, Z. Zhao, Z. Tang, Y. Niu, D. Zhang, Y. Wang and W. Gong, *Analyst*, 2025, **150**, 669–679.

21 C. Sekine, Y. Tsubata, T. Yamada, M. Kitano and S. Doi, *Sci. Technol. Adv. Mater.*, 2014, **15**, 034203.

22 M. Xiao, X. Ren, K. Ji, S. Chung, X. Shi, J. Han, Z. Yao, X. Tao, S. J. Zelewski, M. Nikolka, Y. Zhang, Z. Zhang, Z. Wang, N. Jay, I. E. Jacobs, W. Wu, Y. Han, Y. A. Samad, S. D. Stranks, B. Kang, K. Cho, J. Xie, H. Yan, S. Chen and H. Sirringhaus, *Sci. Adv.*, 2023, **9**, eadg8659.

23 F. Wu, Y. Liu, J. Zhang, S. Duan, D. Ji and H. Yang, *Small Methods*, 2021, **5**, 2100676.

24 H. Sirringhaus, *Adv. Mater.*, 2014, **26**, 1319–1335.

25 N. Balar, J. J. Rech, S. Siddika, R. Song, H. M. Schrickx, N. S. Sheikh, L. Ye, A. M. Bonilla, O. Awartani, H. Ade, W. You and B. O'Connor, *Adv. Funct. Mater.*, 2021, **32**, 2105597.

26 M. Kim, S. U. Ryu, S. A. Park, K. Choi, T. Kim, D. Chung, J. Y. Park and T. Park, *Adv. Funct. Mater.*, 2019, **30**, 1904545.

27 C. Guo, B. Sun and Y. Li, *Polym. Chem.*, 2014, **5**, 5247–5254.

28 Z. Yi, S. Wang and Y. Liu, *Adv. Mater.*, 2015, **27**, 3589–3606.

29 Z. Liu, G. Zhang and D. Zhang, *Acc. Chem. Res.*, 2018, **51**, 1422–1432.

30 I. Kang, H.-J. Yun, D. S. Chung, S.-K. Kwon and Y.-H. Kim, *J. Am. Chem. Soc.*, 2013, **135**, 14896–14899.

31 T. J. Ha, P. Sonar and A. Dodabalapur, *Phys. Chem. Chem. Phys.*, 2013, **15**, 9735–9741.

32 J. Deng, Y. Guo, W. Li, Z. Xie, Y. Ke, R. A. J. Janssen and M. Li, *Nanoscale*, 2023, **15**, 553–561.

33 H. J. Cheon, T. K. An and Y. H. Kim, *Macromol. Res.*, 2022, **30**, 71–84.

This journal is © The Royal Society of Chemistry 2025

J. Mater. Chem. C, 2025, **13**, 18176–18186 | **18185**

34 J. Hong, J. Kim, Z. Li, C. Cong, B. P. Rand, S. Y. Nam, S. H. Kim and Y. H. Kim, *ACS Appl. Electron. Mater.*, 2023, **5**, 4114–4124.

35 X. Su, S. B. Kim, H. Jung, J. Kim, J. Mo, Y. J. Jeong, J. Jang, T. K. An, Y. Kim and J. Jeon, *Macromol. Rapid Commun.*, 2023, **45**, 2300271.

36 G. Yang, C. Di, G. Zhang, J. Zhang, J. Xiang, D. Zhang and D. Zhu, *Adv. Funct. Mater.*, 2013, **23**, 1671–1676.

37 T. Mukhopadhyaya, J. Wagner, H. Fan and H. E. Katz, *ACS Appl. Mater. Interfaces*, 2020, **12**, 21974–21984.

38 D. S. Chung, I. Kang, Y. Kim and S. K. Kwon, *Phys. Chem. Chem. Phys.*, 2013, **15**, 14777–14782.

39 V. Van Tran, G. Jeong, E. Wi, D. Lee and M. Chang, *ACS Appl. Mater. Interfaces*, 2023, **15**, 21270–21283.

40 D. S. Anisimov, A. A. Abramov, V. P. Chekusova, D. Kaplun, E. V. Agina and S. A. Ponomarenko, *ACS Omega*, 2023, **8**, 4649–4654.

41 J. Gayle, S. Roy, S. Gupta, S. Hassan, A. Rao, P. Demingos, K. A. Miller, G. Guo, X. Wang, A. Garg, C. V. Singh, R. Vajtai, J. T. Robinson and P. Ajayan, *ACS Appl. Mater. Interfaces*, 2024, **16**, 2726–2739.

42 J. Yao, C. Yu, Z. Liu, H. Luo, Y. Yang, G. Zhang and D. Zhang, *J. Am. Chem. Soc.*, 2016, **138**, 173–185.

43 Y. Yang, Z. Liu, L. Chen, J. Yao, G. Lin, X. Zhang, G. Zhang and D. Zhang, *Chem. Mater.*, 2019, **31**, 1800–1807.

44 Y. Yang, G. Zhang, H. Luo, J. Yao, Z. Liu and D. Zhang, *ACS Appl. Mater. Interfaces*, 2016, **8**, 3635–3643.

45 A. S. Pavitt, E. J. Bylaska and P. G. Tratnyek, *Environ. Sci.: Processes Impacts*, 2017, **19**, 339–349.

46 G. H. L. Heintges, P. J. Leenaers and R. A. J. Janssen, *J. Mater. Chem. A*, 2017, **5**, 13748–13756.

47 Q. Zou, F. Liu, T. Zhao and X. Hu, *Chem. Commun.*, 2021, **57**, 8588–8591.

48 D. Vaitukaityte, Z. Wang, T. Malinauskas, A. Magomedov, G. Bubniene, V. Jankauskas, V. Getautis and H. J. Snaith, *Adv. Mater.*, 2018, **30**, 1803735.

49 J. Yao, C. Yu, Z. Liu, H. Luo, Y. Yang, G. Zhang and D. Zhang, *J. Am. Chem. Soc.*, 2016, **138**, 173–185.

50 S. Rasool, Q. V. Hoang, D. Van Vu, C. E. Song, H. K. Lee, S. K. Lee, J. C. Lee, S. J. Moon and W. S. Shin, *J. Energy Chem.*, 2021, **64**, 236–245.

51 H. Kong, B. J. Jung and H. E. Katz, *Chem. Mater.*, 2012, **24**, 2621–2623.

52 M. Waldrip, O. D. Jurchescu, D. J. Gundlach and E. G. Bittle, *Adv. Funct. Mater.*, 2020, **30**, 1904576.

53 M. Kádár, Z. Nagy, T. Karancsi and G. Rgy Farsang, *Electrochim. Acta*, 2001, **46**, 1297–1306.

54 S. V. F. Castro, C. V. Silva, J. S. Stefano, E. M. Richter and R. A. A. Munoz, *J. Electroanal. Chem.*, 2020, **877**, 114500.

55 G. Horowitz and P. Delannoy, *J. Appl. Phys.*, 1991, **70**, 469–475.

56 M. M. Marques, L. G. Mourato, M. T. Amorim, M. A. Santos, W. B. Melchior and F. A. Beland, *Chem. Res. Toxicol.*, 1997, **10**, 11.

57 P. R. Erickson, N. Walpen, J. J. Guerard, S. N. Eustis, J. S. Arey and K. McNeill, *J. Phys. Chem. A*, 2015, **119**, 3233–3243.

58 A. V. Afonin, D. V. Pavlov, I. A. Ushakov, E. P. Levanova and G. G. Levkovskaya, *Russ. J. Org. Chem.*, 2013, **49**, 1117–1121.

59 G. Luengo, G. Rojo, R. G. Rubio, M. G. Prolongo and R. M. Masegosa, *Macromolecules*, 1991, **24**, 1315–1320.

60 H. Sirringhaus, *Adv. Mater.*, 2009, **21**, 3859–3873.

61 T. Richards and H. Sirringhaus, *Appl. Phys. Lett.*, 2008, **92**, 023512.

62 S. J. Zilker, C. Detcheverry, E. Cantatore and D. M. De Leeuw, *Appl. Phys. Lett.*, 2001, **79**, 1124–1126.

18186 | *J. Mater. Chem. C*, 2025, **13**, 18176–18186

This journal is © The Royal Society of Chemistry 2025